Symmetric and antisymmetric mass exchanges between the equatorial and off-equatorial Pacific associated with ENSO

Jong-Seong Kug and In-Sik Kang
School of Earth and Environmental Sciences, Seoul National University, Seoul, Korea

Soon-Il An
International Pacific Research Center, SOEST, University of Hawaii at Manoa, Honolulu, Hawaii, USA

Received 3 October 2002; revised 31 May 2003; accepted 17 June 2003; published 29 August 2003.

[1] Mass exchanges in the upper ocean between the equatorial and off-equatorial Pacific Ocean associated with the El Niño/Southern Oscillation (ENSO) are investigated using the National Centers for Environmental Prediction (NCEP) ocean assimilation data. The data show that ENSO-related meridional mass transport in the Northern Hemisphere (NH) is larger than that in the Southern Hemisphere (SH). We found that the antisymmetric characteristics are mainly due to a southward shift of themaximum zonal wind stress anomaly during the ENSO mature phase. The Ekman and geostrophic transports associated with ENSO are separated into symmetric and antisymmetric components. For the symmetric part, the mass divergence over the equatorial Pacific by the geostrophic transport is generally larger than the convergence by the Ekman transport during the El Niño mature phase. Therefore mass is transported from the equator to off the equator at this time. As for the antisymmetric part, the Ekman transport due to antisymmetric wind stress dominates the geostrophic transport so that the mass is transported from the SH to the NH during the El Niño mature phase. The net mass transport in the NH is larger than that in the SH. A theoretical interpretation and intermediate model experiments support these arguments. *INDEX TERMS:* 4522 Oceanography: Physical: El Niño; 4572 Oceanography: Physical: Upper ocean processes; 4512 Oceanography: Physical: Currents; 4504 Oceanography: Physical: Air/sea interactions (0312); 4215 Oceanography: General: Climate and interannual variability (3309); *KEYWORDS:* ENSO, mass exchange, wind stress, antisymmetry

Citation: Kug, J.-S., I.-S. Kang, and S.-I. An, Symmetric and antisymmetric mass exchanges between the equatorial and off-equatorial Pacific associated with ENSO, *J. Geophys. Res.*, *108*(C8), 3284, doi:10.1029/2002JC001671, 2003.

1. Introduction

[2] Since the work of *Bjerknes* [1969], considerable research effort has been devoted to better understanding of El Niño/Southern Oscillation (ENSO) dynamics. Most ENSO studies agree that the ocean provides the memory for longer timescale variations. The ocean memory, manifested by time-varying heat content in the upper ocean, is associated with the slow adjustment processes of the equatorial ocean in response to wind stress forcing. In particular, the recharge oscillator, suggested by *Jin* [1997a, 1997b], emphasizes mass exchanges between the equator and off the equator in order to explain self-sustained ENSO oscillation. The mass transport is determined by quick adjustment of the upper ocean to wind stress forcing but supplies ocean memory, redistributing the ocean mass field [*Jin*, 1997a, 1997b; *An and Kang*, 2000]. Thus investigation of the spatial structure and time evolution of meridional mass transport in the Pacific is important for understanding ENSO dynamics [e.g., *Wyrtki*, 1975, 1985; *Zebiak and Cane*, 1987].

[3] Recent studies using observations [*Meinen and McPhaden*, 2000, 2001], intermediate models [*Perigaud et al.*, 2000; *Cassou and Perigaud*, 2000], and a coupled general circulation model (GCM) [*Yu and Mechoso*, 2001] described the processes of meridional mass exchange analogous to *Jin*'s [1997a, 1997b] recharge oscillator. However, these studies, including Jin's, did not stress the differences between the mass transports in the Northern Hemisphere (NH) and Southern Hemisphere (SH). Rather, most assumed that the mass transport in the SH is equal and opposite that in the NH. However, the observations show distinctive differences between the mass transports in the two hemispheres, as shown in Figure 1. Mass transport in the NH is generally larger than that in the SH during the ENSO mature phase. In this study, we will describe the meridional structure of the mass transport and its related dynamics.

[4] In order to elucidate meridional mass exchange, we introduce the symmetric and antisymmetric components of the mass transport. The symmetric component is defined as having identical poleward (equatorward) transport in the

0148-0227/03/2002JC001671$09.00

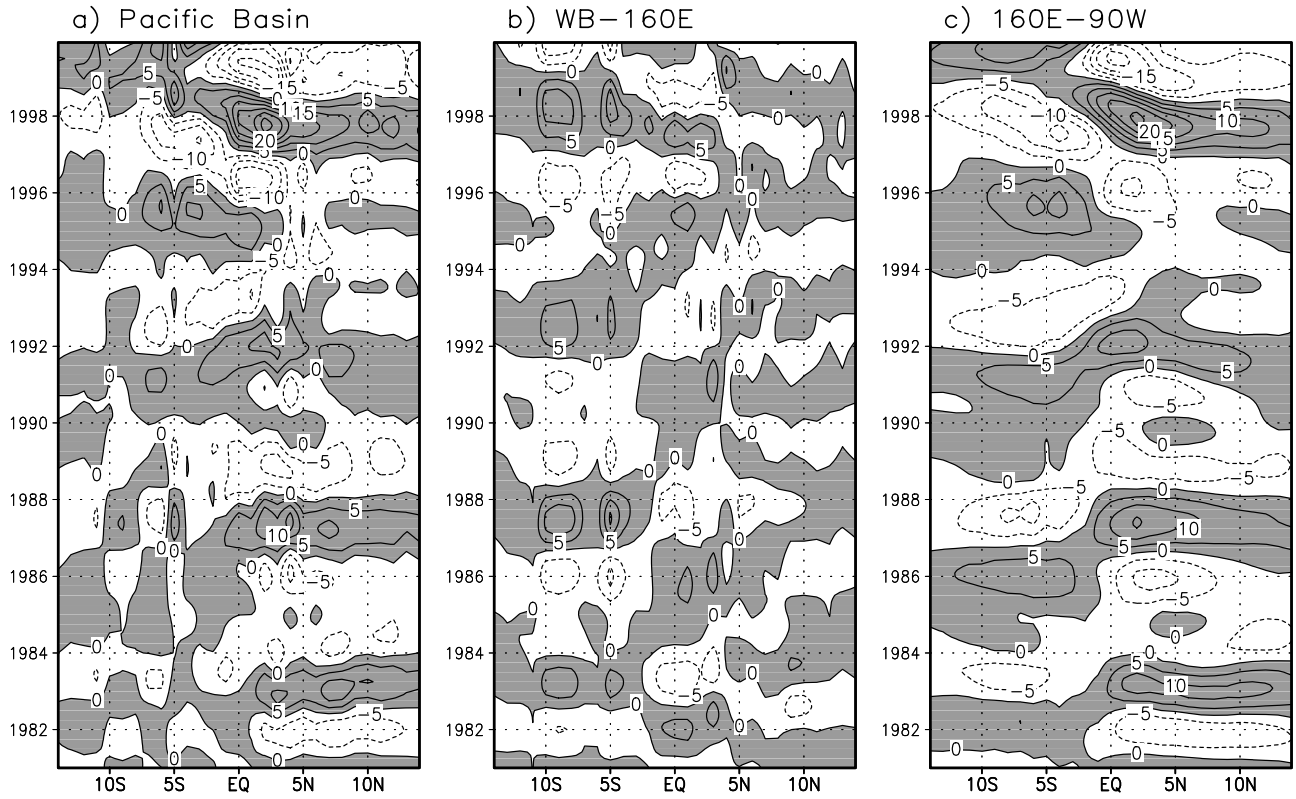

Figure 1. Time-latitude plots of a band-pass-filtered zonal-mean meridional transport calculated from the NCEP ocean assimilation data over (a) all the Pacific basin, (b) the western boundary to 160°E, and (c) 160°E–90°W. Units are 10^9 kg s^{-1}. Positive values are shaded.

two hemispheres, $((V_{NH} - V_{SH})/2)$ which induces mass divergence (convergence) at the equator. Here V_{NH} and V_{SH} are meridional mass transport in the NH and SH, respectively, and are defined in the text. The antisymmetric component encompasses those elements of the flow responsible for mass transport from one hemisphere to the other, $((V_{NH} - V_{SH})/2)$.

[5] Anomalous meridional mass transport in the tropical Pacific Ocean associated with ENSO is related to two mechanisms. One is Ekman transport by direct wind stress forcing, and the other is geostrophic transport related to the east-west pressure gradient [*An and Kang*, 2000]. During the El Niño (La Niña) mature phase, the equatorial westerly (easterly) wind stress anomaly induces anomalous mass convergence (divergence) at the equator by Ekman transport, while the geostrophic current, which is related to the eastward (westward) zonal pressure gradient induced by westerly (easterly) wind stress anomaly, causes anomalous mass divergence (convergence). Thus Ekman and geostrophic transports play opposing roles in relation to the mass exchange associated with ENSO. *An and Kang* [2000] showed in their simple coupled system that when the wind stress is symmetric about the equator, the meridional geostrophic transport is always larger than the Ekman transport in both hemispheres, resulting in a net mass divergence (convergence) about the equator during the El Niño (La Niña) mature phase.

[6] Since both the Ekman and geostrophic flows ultimately depend on the wind stress forcing, the detailed structure of the mass exchange must be strongly related to the location and time evolution of the wind, whose pattern tends to move meridionally during the ENSO evolution [*Rasmusson and Carpenter*, 1982]. Thus wind stress forcing has to be considered in order to investigate the characteristics of the mass exchange associated with ENSO. In this paper, we will describe structures of the mass exchange between the equator and off-equatorial regions, and we demonstrate that a distinctive hemispheric antisymmetry of the mass transport exists. We will also address what causes the antisymmetric mass exchange.

[7] In the following section, we show the characteristics of the mass transport associated with the ENSO using NCEP ocean assimilation data. Especially, symmetric and antisymmetric parts of the mass transport are separated. In section 3, it is claimed that the hemispheric antisymmetry of mass exchange is related to the meridional location of zonal wind stress using a simple theoretical model. Intermediate model experiments are designed to show the role of the zonal wind stress on the antisymmetry of the mass exchange in section 4. The summary and discussion are given in section 5.

2. Ocean Assimilation Data Analysis

[8] The data utilized are NCEP ocean assimilation data for January 1980 to October 2000 [*Ji et al.*, 1995; *Behringer et al.*, 1998; *Vossepoel and Behringer*, 2000]. Observed surface and subsurface ocean temperatures as well as

satellite altimetry sea level data from TOPEX/POSEIDON were assimilated into a Pacific basin ocean general circulation model. The model was forced with weekly mean surface winds and heat fluxes of NCEP operational atmospheric analyses of surface winds.

[9] *Behringer et al.* [1998] compared equatorial current data with those of observation and the previous version (RA5 analysis). They showed that the average surface currents are closer to the averaged current estimates, from surface drifter for 1978–1994 shown by *Acero-Schertzer et al.* [1997], as compared to previous analysis. Recently, *Vossepoel and Behringer* [2000] showed that the assimilation of TOPEX/POSEIDON observations improves dynamic height simulation without degrading the temperature field. They demonstrated that the application of altimetry improves the mean salinity and it leads to a more accurate calculation of the ocean density structure. These improvements allow a better simulation of the ocean currents. Based on previous studies, we used the assimilation data instead of intermittent and coarse-resolution-observed ocean current in order to analyze and understand the transport variations associated with ENSO.

[10] In this study, the zonal-mean meridional mass transport is calculated by zonally and vertically integrating the meridional current across the width of the Pacific:

$$\text{mass transport} : V = \int_{sfc}^{200\text{m}} \int \rho v \, dx \, dz.$$

[11] The vertical integration is taken from the surface to 200 m, where it includes the equatorial thermocline. We varied the integration depth between 150 and 250 m, but our main conclusions were not sensitive to the maximum depth.

[12] In order to show the interannual variation of mass transport, we removed the mean seasonal cycle of the ocean variables. Hereafter, we will focus on the anomalous fields. Figure 1 shows time-latitude plots of zonal-mean meridional mass transport. In order to focus on interannual variation, a band-pass filter for 18–84 months was applied to the data. Interannual variation of the meridional mass transport is mainly related to the major ENSO events, as shown in Figure 1a. However, the mass exchanges tend to mainly appear in the NH, except during the early 1990s. The meridional mass transport can be subdivided into the flow at the western boundary (Figure 1b) and the ocean interior (Figure 1c), 160°E–90°W. We found that the eastern boundary transport is relatively small. If the wind stress forcing and western boundary were symmetric, the same current would be expected north and south of equator at the western boundary. However, as shown in Figure 1b, the western boundary current in the SH is stronger than that in the NH due to an antisymmetric western boundary such as the slanted coastal boundary of New Guinea Island.

[13] In spite of removing the boundary effect, hemispheric antisymmetry of the meridional mass transport still exists (Figure 1c). In the ocean interior, mass transport in the NH is stronger than in the SH over most periods. This suggests that there is another mechanism that causes antisymmetric mass exchange besides the antisymmetric western boundary.

[14] Figure 2 shows Lagged Linear Regression (LLR) of the zonal-mean meridional mass transport with respect to the NINO3.4 sea surface temperature (SST) (170°–120°W and 5°S–5°N), which represents the evolution of the mass transport associated with the ENSO. The LLR is defined as follows:

$$\text{LLR} = \frac{\frac{1}{n}\sum_{t=1}^{n} V(t - \text{lag})\text{NINO3.4}(t)}{\sigma^2_{\text{NINO3.4}}},$$

where n is the number of time record. As shown in Figure 2a, between lags −12 and +12 months, indicating 1 year before to 1 year after the mature phase of ENSO, the mass transports are poleward in both hemispheres so as to discharge the upper ocean mass from the equator [*Jin*, 1997a, 1997b], but the amplitude in the NH is three times larger than that in the SH. The node latitude of maximum mass transport is located slightly south of the equator. The latitudes of the maximum mass transport are about 5°S in the SH, while it is about 3°N in the NH.

[15] As shown in Figure 2b, the western boundary currents act to reduce the rate of discharge of mass during warm event. The boundary current in the SH is much stronger than that in the NH, which is in agreement with the previous discussion. The meridional currents in the ocean interior have greater strength and overwhelm the boundary current (Figure 2c); the net mass transport during warm events is divergent poleward, as shown in Figure 2a and as shown by *An and Kang* [2000]. Note that the interior meridional current at these times also shows the antisymmetric mass exchange between the two hemispheres. We will propose that an antisymmetric spatial distribution of the wind stress can cause the antisymmetric mass exchange. In addition, as shown in Figure 2, the mass transport due to the interior current overcompensates that due to the boundary current, so hereafter our focus will mostly be on the interior current effects.

[16] Mass transport in the upper ocean is mainly determined by geostrophic and Ekman currents. To investigate the effect of each transport, we separately calculate the geostrophic and Ekman transports using the NCEP ocean assimilation data. The geostrophic current is calculated by the following procedures: (1) calculate the density using salinity and seawater temperature following *Gill* [1982], (2) calculate the zonal pressure gradient by vertically integrating the density field from a reference depth, 500 m, assuming no horizontal pressure gradient at this level, and (3) finally calculate the geostrophic current using the pressure gradient and density field. Note that *Meinen and McPhaden* [2001] calculated the geostrophic transport using the dynamic height anomalies from the Australian Bureau of Meteorology Research Centre (BMRC) subsurface temperature data [*Smith*, 1995]. Although dynamic height is determined by temperature and salinity, the BMRC climatology is based on expendable bathythermograph (XBT) data that lack salinity information. Instead, they utilized the temperature-salinity (T-S) approach of *Meinen and Watts* [2000] in order to consider the salinity

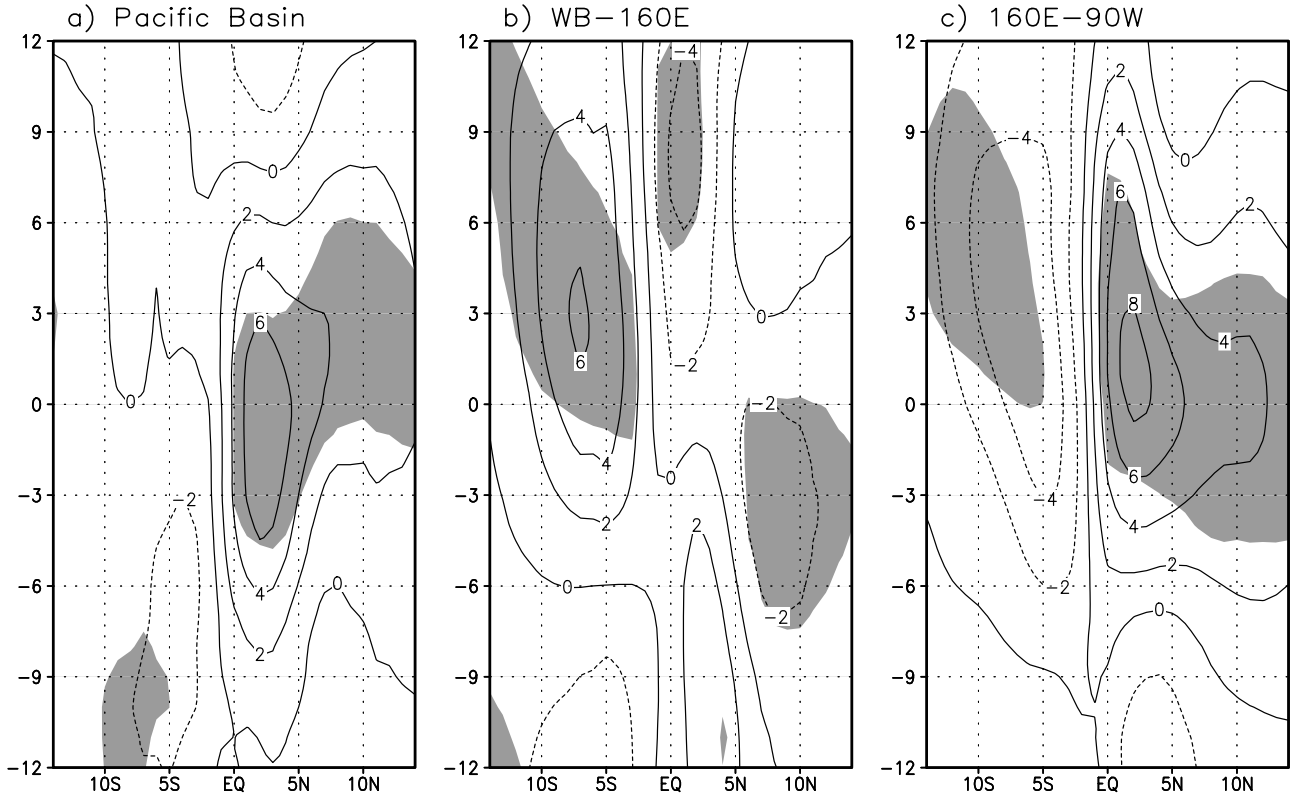

Figure 2. LLR of the meridional mass transport with respect to the NINO3.4 SST over (a) all the Pacific basin, (b) the western boundary to 160°E, and (c) 160°E–90°W. The *Y* axis denotes the lag time in months, with positive values indicating that the NINO3.4 SST leads the meridional mass transport. Units are 10^9 kg s^{-1}. The shaded regions denote areas where the correlation coefficient is significant at the 95% confidence level.

effect. In this study, however, we obtained the geostrophic current using the temperature and salinity data. Nevertheless, the salinity effect on the geostrophic current turns out to be relatively small.

[17] In order to investigate the detailed features of the meridional mass transport during the ENSO mature phase, we constructed a vertical cross section of the meridional current at 4°N and 4°S using a linear regression method with respect to the NINO3.4 SST (Figure 3). The strong meridional flow during the mature phase of ENSO appears near 50-m depth at 4°N and at 100-m depth at 4°S. It is interesting that the geostrophic current is relatively stronger in the SH (Figures 3c and 3d), while the total mass transport in the NH is larger than that in the SH (Figures 3a, 3b, and 2a). The equatorward current at 4°N is confined in a very shallow surface layer of the central Pacific. In contrast, the corresponding equatorward current at 4°S extends down to 50 m across the whole Pacific interior. These equatorward flows are associated with the Ekman transport induced by the westerly wind stress anomaly. The Ekman transport in the SH is stronger than that in the NH. In the SH, the Ekman transport is almost compensated by the geostrophic transport so that total meridional mass transport is small as compared to that in the NH. The results indicate that the hemispheric antisymmetry in mass exchange is related to the asymmetry of the Ekman transport.

[18] Figure 4 shows a linear regression pattern of SST, zonal wind stress, and sea level with respect to the NINO3.4 SST. During the ENSO mature phase, the SST anomaly tends to be located slightly south of the equator. This is related to the climatological mean upwelling, whose axis is displaced south of the equator in the eastern Pacific. Therefore the SST anomaly in the SH is somewhat larger due to the vertical advection of the anomalous subsurface temperature by the mean upwelling. The corresponding SST pattern can accompany a southward migration of the zonal wind stress (Figure 4b).

[19] However, it is interesting that the maximum of the wind stress is located farther to the south than that of the SST pattern, as shown in Figure 4. This implies that there is another reason for the southward shift of the maximum wind stress besides the antisymmetric SST anomaly. This wind stress pattern may be related to the climatological mean SST. The ENSO mature phase tends to occur during the boreal wintertime when the warm pool is expanding into the southwestern-to-central Pacific. At the same time, the warm pool region in the NH is shrinking [*Harrison and Vecchi*, 1999]. Because tropical convection preferentially occurs over the areas of warmest SST, convection anomalies and their resultant wind stress anomalies shift south.

[20] Since the equatorial sea level distribution is mainly determined by the Sverdrup response to wind stress forcing

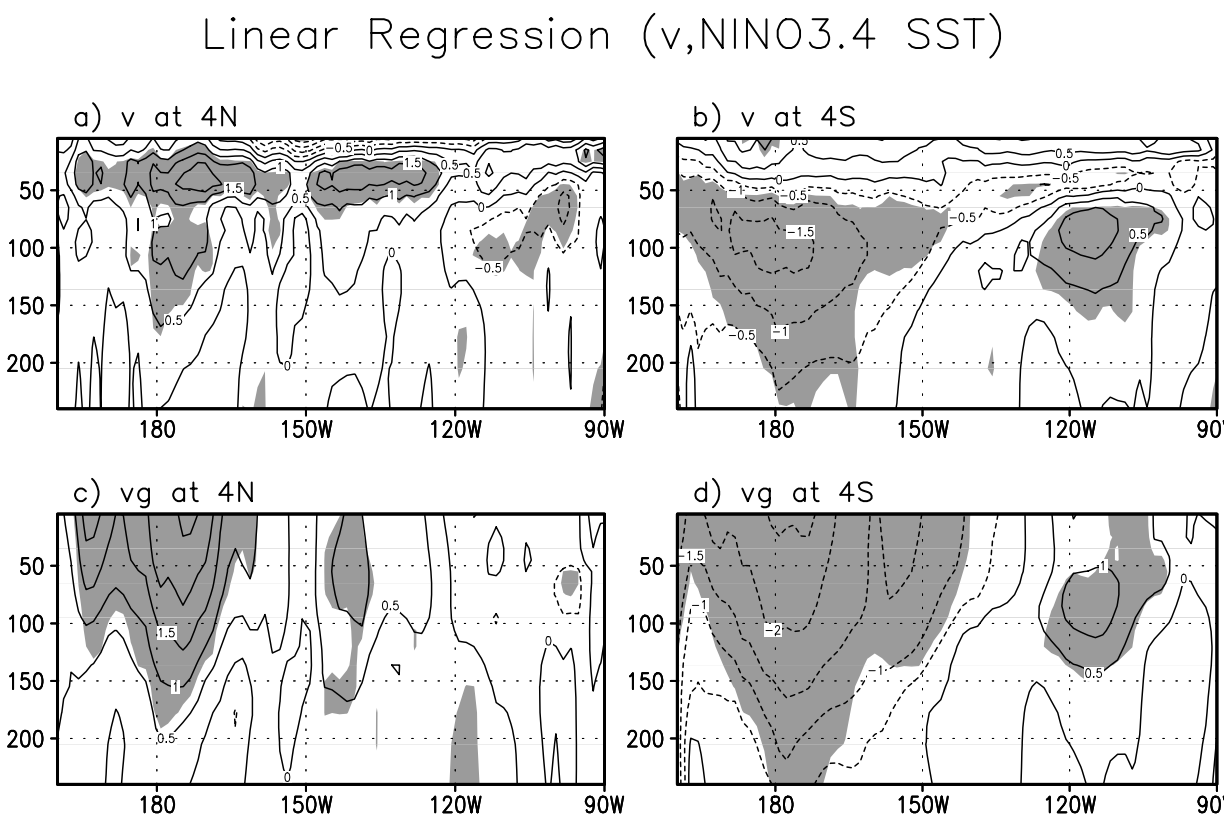

Figure 3. Linear regression of (a and b) the observed meridional current and (c and d) the geostrophic meridional current at 4°N and 4°S with respect to the NINO3.4 SST, respectively. Units are in centimeters per second. The shaded regions denote areas where the correlation coefficient is significant at the 95% confidence level.

[*Cane and Sarachick*, 1981], the maximum sea level anomaly is also shifted slightly south with respect to the equator (Figure 4c). In addition, large negative sea level anomalies exist in the southwestern Pacific. These negative sea level anomalies are generated by strong wind stress curl by the southward shift of the zonal wind stress. Accordingly, the zonal slope of the sea level is steeper in the SH so that the geostrophic current is stronger in the SH, as shown in Figure 3.

[21] Thus the southward shift of the wind stress pattern causes an enhancement of both the Ekman and geostrophic currents in the SH, which flow in opposite directions to each other. In that situation, the net mass transport of the NH might be larger than that of the SH if the Ekman transport is more affected by the southward shift of the wind stress compared to that of the geostrophic transport. In order to examine quantitatively the impact of the southward shift of wind stress, we separately calculated the symmetric and antisymmetric parts of the mass transport, as shown in Figure 5. These results are obtained from a linear regression with respect to the NINO3.4 SST. The geostrophic transport is calculated based on that of Figure 3, and the Ekman transport is calculated from the wind stress using the simple formula, $V_{\mathrm{Ekman}} = -\tau/\rho f$ [*Gill*, 1982].

[22] For the symmetric part, the magnitude of the geostrophic transport is larger than that of the Ekman transport. For example, at latitude 5° the magnitude of the geostrophic current is about 2.5 times larger than the Ekman transport (Figure 5a). The observed symmetric part, calculated from the assimilated meridional current, indicates mass divergence in the equatorial region during the El Niño mature phase, consistent with the recharge oscillator proposed by *Jin* [1997a, 1997b] and *An and Kang* [2000].

[23] For the antisymmetric part, both geostrophic and Ekman transports are maximum near latitude 5°. However, the magnitude of the Ekman transport is larger than that of the geostrophic transport, and so the net transport (Ekman transport plus geostrophic transport) is northward at all latitudes during the ENSO mature phase. The observed antisymmetric part also indicates northward transport in both hemispheres. These results support the view that the hemispheric asymmetry of mass transport associated with ENSO results from the antisymmetric Ekman transport due to the southward shift of the wind stress.

[24] However, the antisymmetric total transport is not well captured by the diagnosed geostrophic plus Ekman transport, especially near the equator where the geostrophic constraint is not valid, i.e., the Sverdrup transport cannot be explained by the geostrophic plus Ekman transport near the equator. However, it is conceivable that the Sverdrup transport due to the antisymmetric wind stress directly explains some parts of the observed northward transport near the equator. Since the center of the wind stress is shifted to the south about the equator, the antisymmetric

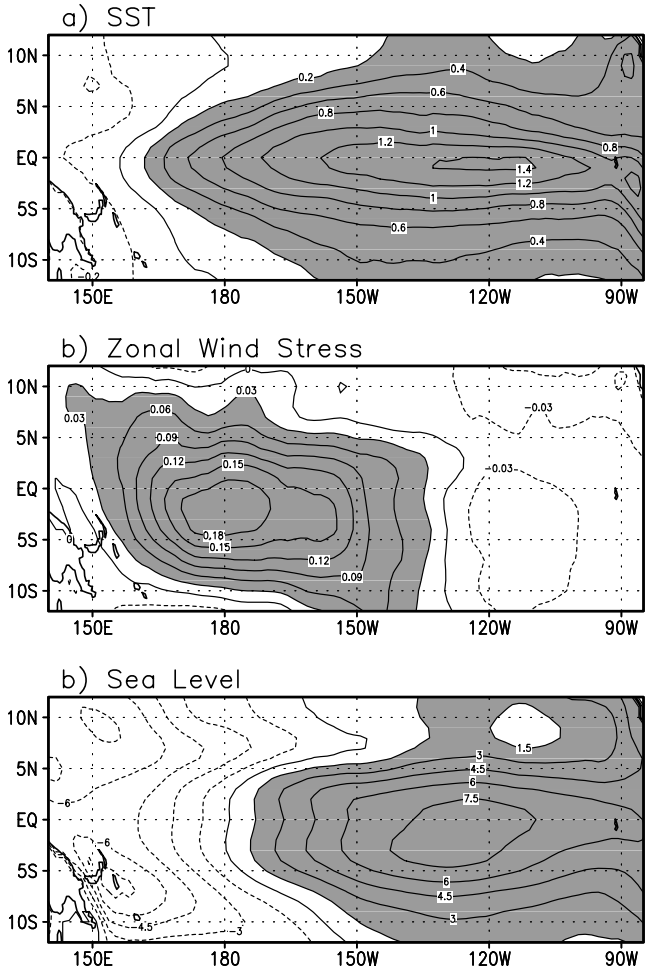

Figure 4. Same as in Figure 3 except for (a) SST, (b) zonal wind stress, and (c) sea level.

part of the wind stress is easterly (westerly) north (south) of the equator. Therefore the wind stress curl is counterclockwise at the equator so that the Sverdrup transport is northward, as shown in Figure 5b. This indicates that near the equator the antisymmetric mass transport is partly contributed by the Sverdrup transport due to the antisymmetric wind stress, as well as the antisymmetric Ekman transport. In the next section, we will show, using a simple theoretical model, that the antisymmetric wind stress can generate northward Sverdrup transport across the equator.

3. Simple Theoretical Model

[25] In section 2, we documented hemispheric mass exchange associated with ENSO related to the location of the zonal wind stress pattern. In this section, we will examine the steady state response of the ocean to the wind forcing during the mature phase of ENSO under a simple context. In particular, we will address how the meridional shift of the zonal wind stress affects the Ekman and Sverdrup transports.

[26] The upper layer equatorial ocean adjusts quickly to a given large-scale wind forcing through the fast equatorial waves [*Cane and Moore*, 1981; *Jin*, 1997a, 1997b]. Thus the Sverdrup balance near the equator is almost simultaneously achieved [*Jin*, 1997a, 1997b; *An and Kang*, 2001]. For a given wind stress, we have the Ekman transport equation and the Sverdrup balance equation,

$$\text{Ekman transport} : \rho v_e H_1 = \frac{-\beta y \tau_x}{\left(r_s^2 + \beta^2 y^2\right)}$$
$$\text{Sverdrup transport} : \rho v_s H = \frac{-1}{\beta}\frac{\partial \tau_x}{\partial y}, \qquad (1)$$

where H_1 and H denote the mean Ekman layer depth and the thermocline depth, respectively. The formula of the Ekman transport is adopted from the model of *Zebiak and Cane* [1987]. r_s is a surface layer friction coefficient. For simplicity, effect of meridional wind stress is neglected in both equations. We explore the response to an identical zonal wind stress, with a spatial pattern resembling the dominant structure during the ENSO mature phase as shown in Figure 4b:

$$\tau_x(x,y) = A(x)\exp\left[-\frac{(y+y_0)^2}{Y_c^2}\right], \qquad (2)$$

where $A(x)$ is a zonal structure function that relates to the pattern of the atmospheric heating in the equatorial region. Y_c is the meridional length scale of the zonal wind stress, and y_0 denotes the latitudinal displacement of the maximum wind stress from the equator. When y_0 is positive, the pattern of the wind stress is shifted south about the equator. The antisymmetry of the wind stress can be controlled by changing the value of y_0. In this study, we choose the value of y_0 as 3 latitudinal degrees based on Figure 4b.

[27] Using equations (1) and (2), we calculate the Ekman and Sverdrup transports driven by this wind patch. As shown in Figure 6a, the model Ekman and Sverdrup transports are very similar to the observations (Figure 2c). For instance, the Sverdrup transport in both hemispheres is maximized at 2°–3°N and 6°S, respectively, and in its magnitude the Sverdrup transport in the NH is larger than in the SH. As in Figure 5, the northward Ekman transport in the SH is larger than the southward Ekman transport in NH.

[28] Next, we examine separately the mass transport due to the symmetric wind and antisymmetric wind components. To do so, we verify whether a slight shift of a wind patch can cause a large difference between the mass transport in the NH and that in the SH. For the detailed processes of equations, the reader is referred to the Appendix A.

[29] By substituting equation (2) into equation (1), the Ekman and Sverdrup transports due to the symmetric wind stress can be expressed as follows:

$$\text{Ekman} : \frac{-\beta y}{r_s^2 + \beta^2 y^2}\tau_s = \frac{-\beta y}{r_s^2 + \beta^2 y^2} B \exp\left[-\frac{y^2}{Y_c^2}\right]$$
$$\text{Sverdrup} : \frac{2y}{\beta Y_c^2}\tau_s = \frac{2y}{\beta Y_c^2} B \exp\left[-\frac{y^2}{Y_c^2}\right]. \qquad (3)$$

[30] The above equations show that the symmetric westerly (easterly) wind stress component drives mass convergence (divergence) in the Ekman layer and mass divergence

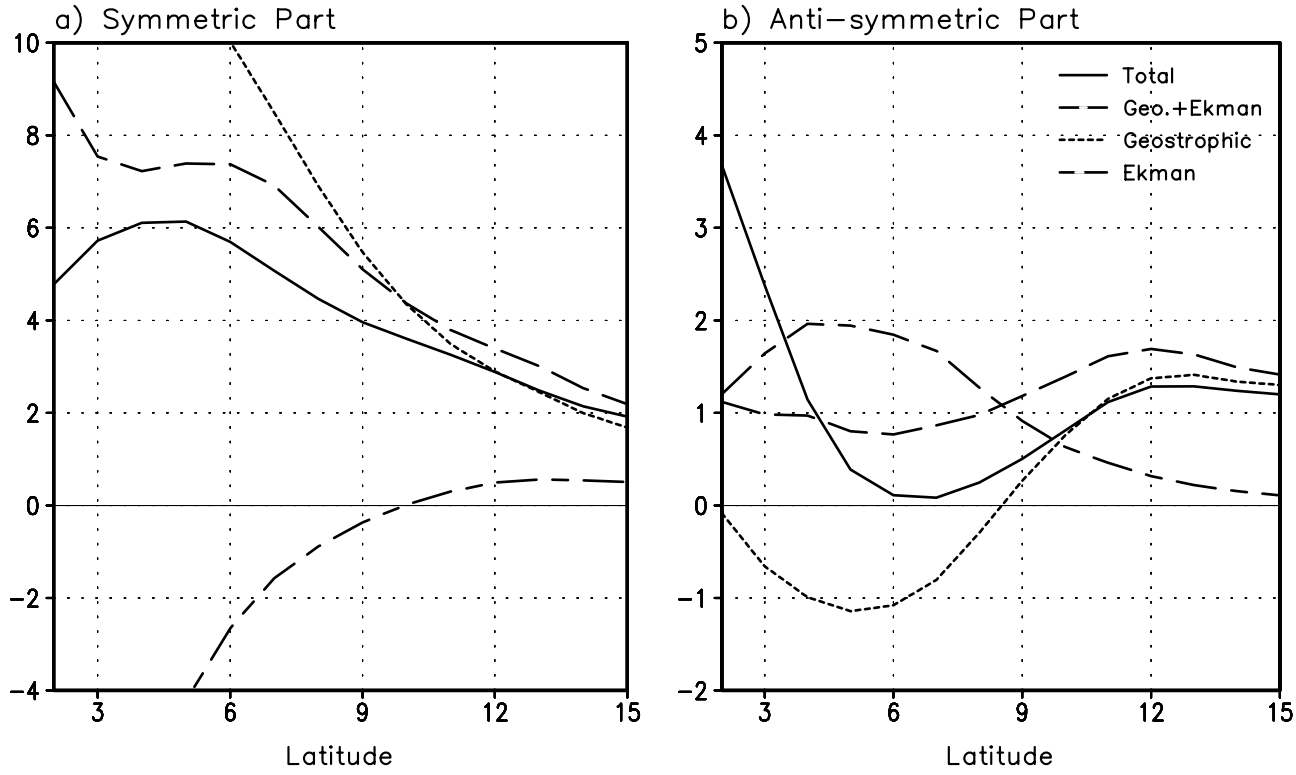

Figure 5. Linear regression of (a) the symmetric part and (b) the antisymmetric part of the zonally averaged mass transport over 160°E–90°W with respect to the normalized NINO3.4 SST. Solid line, short dashed line, and long and short dashed lines indicate the observed, geostrophic, and Ekman transports, respectively. Long dashed line denotes the geostrophic plus the Ekman transport. Units are 10^6 kg s^{-1}.

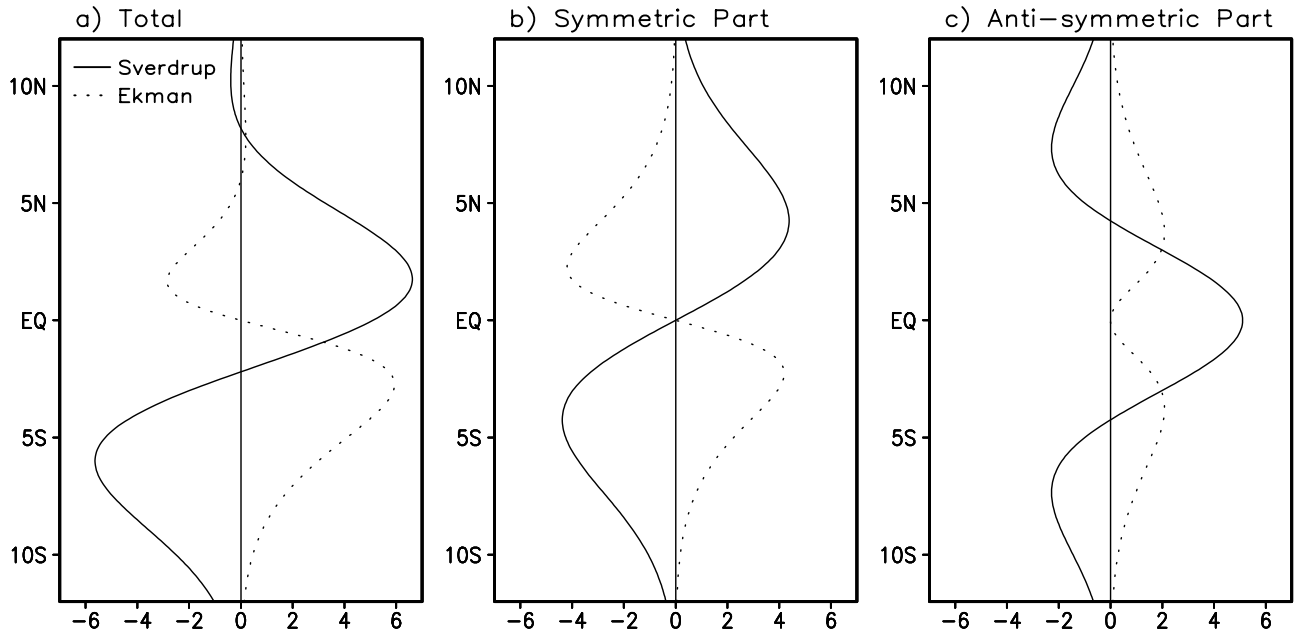

Figure 6. Latitudinal structures of the (a) total mass transports, (b) symmetric mass transports, and 7 (c) antisymmetric mass transports for the Ekman (dotted line) and Sverdrup (solid line) components from equation (1). The units are arbitrary.

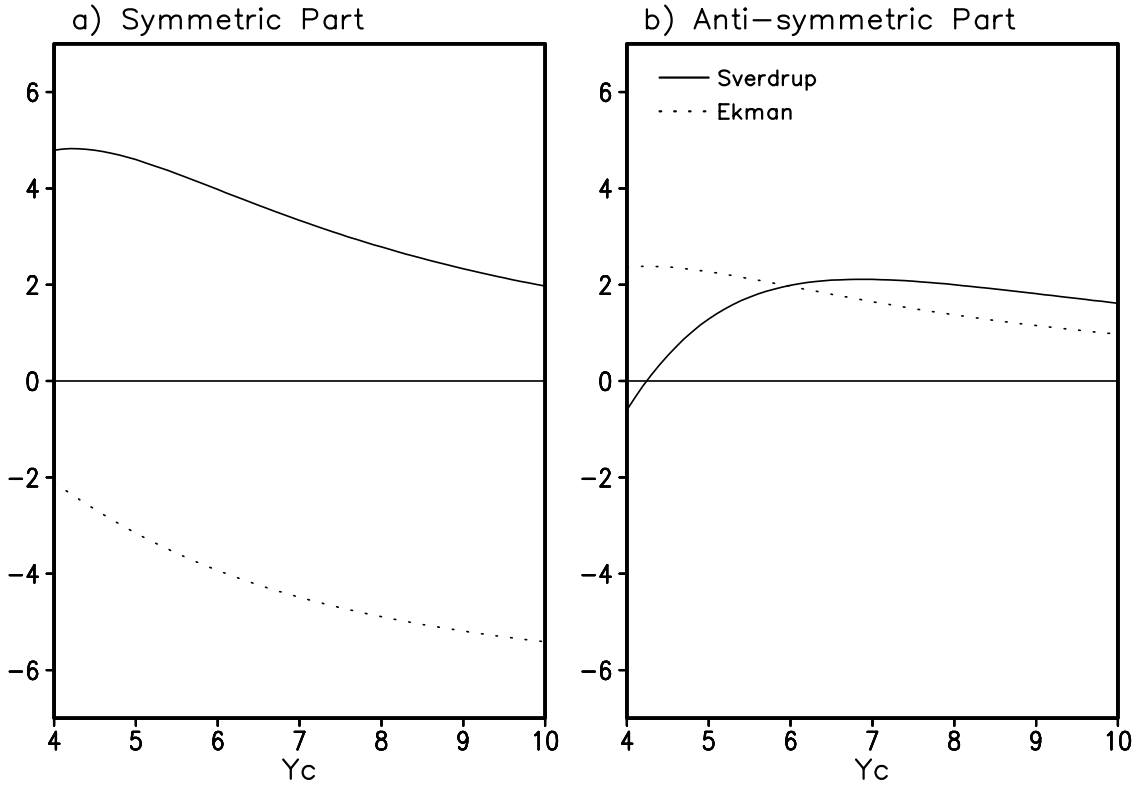

Figure 7. Structure of the (a) symmetric and (b) antisymmetric mass transports by the Ekman (dotted line) and Sverdrup (solid line) component at 3°N from equation (2) with various values of Y_c.

(convergence) by the Sverdrup transport over the equatorial region.

[31] We evaluated equation (3) with the values of $Y_c = 6°$ and $r_s = 1.5\ \mathrm{d}^{-1}$. Figure 6b shows the latitudinal magnitudes of the mass transport induced by the Ekman and Sverdrup mechanisms. As expected, the Sverdrup transport is always positive. It indicates that the water mass is transported from the equatorial region to off-equatorial regions during the El Niño mature phase, and the Ekman transport opposes the mass divergence in the equatorial region. Note that the Sverdrup transport is largest at 4°N. These features are consistent with the observations, as shown in Figure 5b.

[32] Next, the Ekman and the Sverdrup transports due to the antisymmetric wind forcing are expressed as follows:

$$\text{Ekman transport}: \frac{\beta y}{r_s^2+\beta^2 y^2}\tau_a = \frac{\beta y}{r_s^2+\beta^2 y^2}\left(\frac{y_0 y}{Y_c^2}\right)\cdot B\,\exp\left(-\frac{y^2}{Y_c^2}\right)$$

$$\text{Sverdrup transport}: -\left(\frac{2y}{\beta Y_c^2}-\frac{1}{\beta y}\right)\tau_a = -\left(\frac{2y}{\beta Y_c^2}-\frac{1}{\beta y}\right)\left(\frac{y_0 y}{Y_c^2}\right)\cdot B\,\exp\left(-\frac{y^2}{Y_c^2}\right). \quad (4)$$

[33] The equations indicate that the Ekman transport due to the antisymmetric wind forcing is always positive in both hemispheres, when westerly wind stress anomaly is shifted south of the equator. On the other hand, the direction of the Sverdrup transport can be changed according to the latitude and the meridional length scale of the wind stress. Equation (4) reveals that the Sverdrup transport due to the antisymmetric wind forcing within a latitudinal band of $-Y_c/2^{1/2} < y < +Y_c/2^{1/2}$ is positive and outside of that band is negative. For example, when $Y_c = 6°$, between 4.2°S and 4.2°N, the Sverdrup flow due to the antisymmetric wind forcing is from the SH to the NH and those in the other regions is southward (Figure 6c).

[34] Note that the Sverdrup transport in equation (4) is similar to that of the symmetric part except for the additional term $(-\tau_a/\beta_y)$ The additional term has the same sign as the Ekman transport, so that it acts to reduce a southward Sverdrup transport when a westerly wind stress anomaly exists.

[35] Figure 7 shows the transports at 3°N for various meridional length scales of the wind stress (Y_c). The Sverdrup mass transport gradually decreases as the meridional length scale of wind stress increases, which is also clearly understood from the Sverdrup equation of equation (4), the denominator includes Y_c^2. Therefore the recharge/discharge processes of the equatorial water mass during the mature phase of El Niño become slower as the meridional length scale of wind stress becomes larger. The slower mass exchange may result in an increase of the ENSO period because it may cause a slow phase transition [*An and Kang*, 2001].

[36] The relationship between the meridional scale of surface wind and the ENSO period has been demonstrated by observations [*Wang et al.*, 1999], a hybrid coupled model [*Kirtman and Zebiak*, 1997; *Kirtman*, 1997], and a theoretical model [*Wang and Fang*, 1996]. Their argument is somewhat different from ours. These authors suggest that a larger meridional scale of the wind stress favors the generation of the higher meridional modes of the ocean

Rossby waves that propagate westward at a slower speed, which results in a longer period. Our explanation does not explicitly require the Rossby waves, and it only refers to the balanced state, which is a reasonable approximation in the tropical Pacific Ocean. Intrinsically, both the remote effect by Rossby waves and the local response to the direct wind forcing are included in our speculation.

[37] In the case of the Ekman and Sverdrup transport due to the antisymmetric wind forcing, if the meridional length scale is larger than 4.2 latitudinal degrees, the Sverdrup transport of the antisymmetric part is northward. This result indicates that the antisymmetric part of the mass transport represents a northward transport in the realistic range of Y_c.

[38] So far, we have calculated the equation by assuming a 3° southward shift of the wind stress. In order to examine the sensitivity of the location of the wind stress we calculate the variation of the mass transport with respect to various wind stress locations (y_0). As the location of the wind stress is gradually shifted south from the equator in the realistic range (0°–5°S), the Ekman and Sverdrup transports due to the antisymmetric wind forcing gradually increase (not shown). Also, the difference between the Ekman and geostrophic transports increases so that the hemispheric antisymmetry of mass transport becomes larger. This indicates that the meridional location of zonal wind stress is an important factor influencing the ENSO evolution by controlling the mass exchange between the equator and off-equator regions.

[39] A note of caution should be sounded regarding the simple equation used in this section to derive the forced steady solution. While the meridional transport in the ocean interior basin is locally in quasiequilibrium with the wind stress forcing on ENSO timescales, the transports associated with boundary current are not due to the delay time of Rossby wave propagation. Therefore the model can be validly compared to observations in the central Pacific, where wind stress forcing is strongest. Here the latitudinal structure of the mass exchange calculated from the simple equation shown in Figure 6 is very similar to observed transports in the central Pacific. However, the results cannot be applied to other regions where local wind stress forcing is weak and boundary effects exist.

4. Intermediate Model Experiments

[40] In previous sections, we showed the characteristics of the hemispheric antisymmetry of mass exchange associated with ENSO and emphasized that the antisymmetric features are mainly attributed to the southward shift of the zonal wind stress. In this section, we carried out numerical experiments with an intermediate coupled model in order to explore the role of the meridional shift of the zonal wind stress location on mass exchange between the equator and off-equator regions. We used the Lamont ocean model [*Zebiak and Cane*, 1987] and an empirical atmospheric model adopted from the work of *Kang and Kug* [2000]. The atmospheric model is statistically constructed by Singular Value Decomposition (SVD) analysis of the observed wind stress and SST anomalies. In model experiments, the atmospheric model produces zonal wind stress from the model-produced SST using empirical relation.

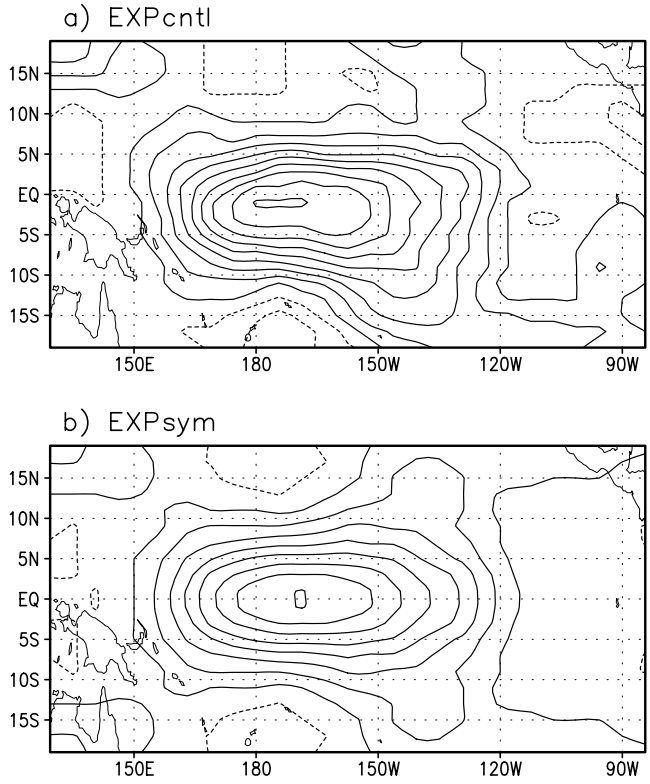

Figure 8. Wind stress patterns used in intermediate model experiments: (a) EXPcntl obtained from SVD first mode and (b) EXPsym calculated from Figure 8a. Units are arbitrary.

Thus the pattern of the wind stress is fixed, but its magnitude is varied with magnitude of the SST anomaly. The ocean model has a rectangular basin so the geometry at the western boundary is symmetric with respect to the equator, and therefore the antisymmetric boundary current due to geometry does not occur in these simulations.

[41] For the control experiment, the first eigenmode representing the zonal wind stress during the ENSO mature phase is adopted as the atmosphere model (hereafter "EXPcntl"). It is noted that the location of maximum zonal wind stress is shifted to the south from the equator (Figure 8a). The coupled model was integrated for 100 years. The model simulates a nearly regular ENSO-like oscillation with a timescale of about 4 years.

[42] In order to examine the role of the southward shift of zonal wind stress, we designed another experiment, which only considered the symmetric wind stress pattern in a statistical atmospheric model (hereafter "EXPsym"). The spatial pattern of the zonal wind stress for EXPsym is shown in Figure 8b. EXPsym was also integrated for 100 years, and its results are compared with those of EXPcntl. The experimental designs of the EXPcntl and EXPsym are exactly the same, except in the pattern of zonal wind stress. Thus it is expected that the differences between the two experiments arise mainly from the differences in the wind stress patterns.

[43] Figure 9 show the linear regression patterns of SST, the meridional current, and the Ekman current with respect to the NINO3.4 SST obtained from EXPcntl and EXPsym.

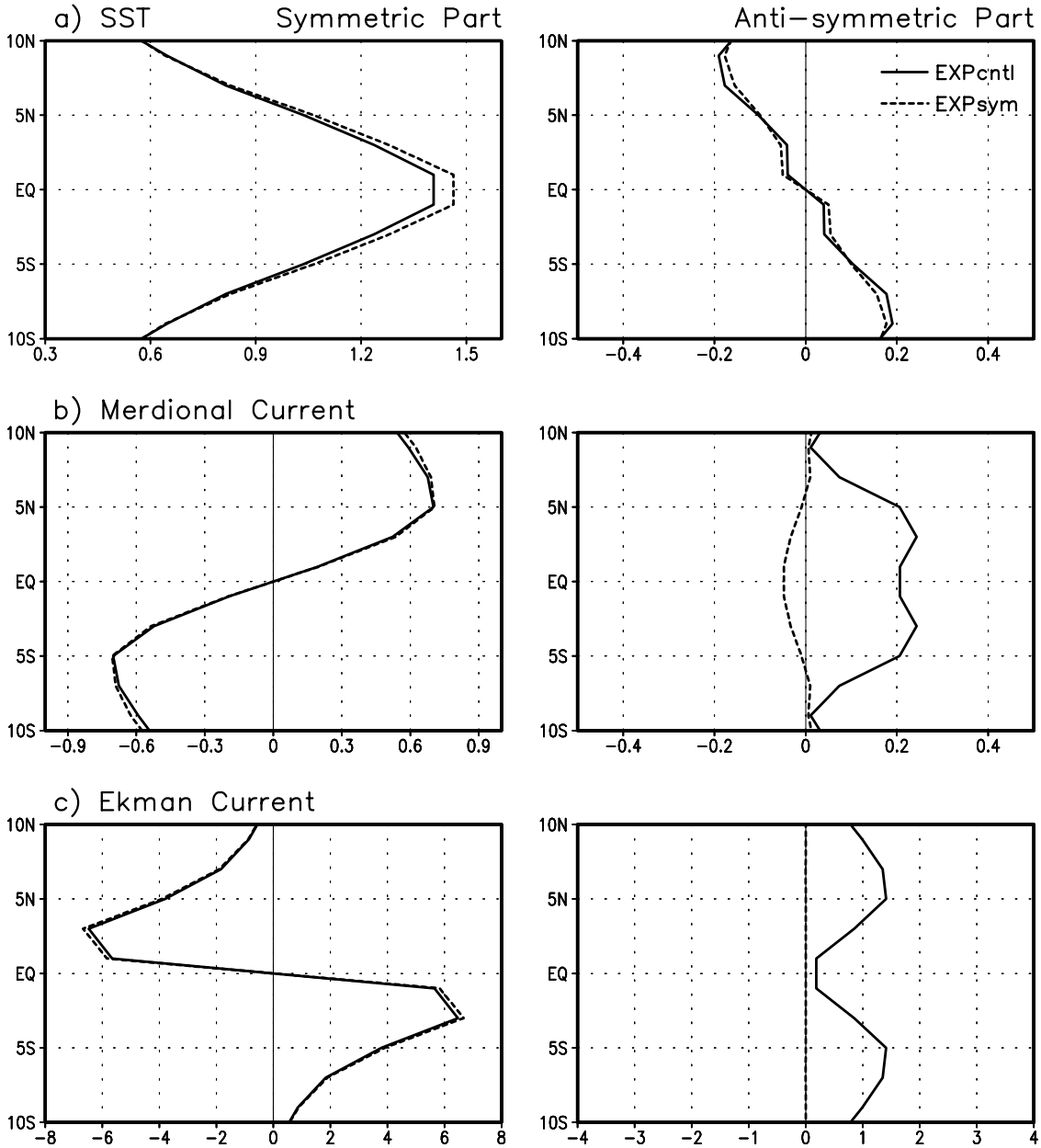

Figure 9. Linear regression of EXPcntl (solid line) and EXPsym (dotted line) results with respect to normalized NINO3.4 SST. (a) SST averaged over 150°–90°W, (b) meridional current of the upper ocean averaged over 160°E–90°W, and (c) Meridional Ekman current averaged over 160°E–90°W. First, third, and fifth panels are the symmetric parts, and second, fourth, and sixth panels are the antisymmetric parts.

For easy comparison, we separate each regression pattern into its symmetric and antisymmetric parts. In both EXPcntl and EXPsym, the antisymmetric part of the SST field is located to the south of the equator (Figure 9a). This suggests that the asymmetry of SST may not be related to the antisymmetry of wind stress but is related to the basic state of the ocean fields such as the climatological upwelling, as mentioned in section 2. However, regarding the symmetric part, the SST magnitudes of EXPsym are slightly larger than those of EXPcntl. The thermocline depth anomaly in the western Pacific also appears to be larger in the SH as compared to the NH, as is the case in the ocean assimilation data (not shown).

[44] The meridional current patterns are shown in Figure 9b. In the case of the EXPcntl, the mass transport in the NH is larger than that in the SH. The antisymmetric mass transport mainly results from the difference in the Ekman transport between the two hemispheres (Figure 9c). Owing to the location of wind stress, the Ekman transport is stronger in the SH. Although the geostrophic current is also larger in the SH (not shown), the mass transport is larger in the NH due to the antisymmetric wind stress. On the other hand, the meridional currents in the upper ocean and the Ekman currents are nearly symmetric about the equator when the zonal wind stress is symmetric, as shown in Figures 9b and 9c.

[45] In spite of the simplicity of the model, EXPcntl captured the major antisymmetric characteristics well. However, when the wind stress pattern was symmetric, the antisymmetric characteristics vanished, except for SST. This verifies that the hemispheric antisymmetry of the ocean variables results from a southward shift of the wind stress, as suggested in the previous section.

5. Summary and Discussions

[46] In this study, the characteristics of the mass transport associated with the ENSO were investigated. The hemispheric antisymmetry of the mass exchange between the equator and off-equator regions is prominent. In a zonal-mean sense, mass exchange occurs mainly in the NH and is nearly zero in the SH. This antisymmetric mass exchange is mainly attributed to the southward shift of the wind stress that produces the antisymmetric meridional mass transport and the north-south antisymmetric geometry at the western boundary that generates a relatively stronger western boundary current in the SH than that in the NH. Through the analysis of the NCEP ocean assimilation data and the model experiments, we revealed that the southward shifted wind stress can induce much strong antisymmetric Ekman transport than geostrophic transport, so the total mass transport becomes smaller in the SH. Regarding the antisymmetry of the western boundary current, this might be due to a strong return flow around New Guinea in the SH.

[47] Our present findings naturally raise crucial questions regarding what causes the meridional shift of wind stress and how the antisymmetric mass exchange influences the ENSO frequency and evolution. Recently, *Harrison and Vecchi* [1999] argued that the termination of the recent El Niño is related to a late-in-the-year shift of El Niño equatorial westerly wind anomalies, from symmetric about the equator to south of the equator. They emphasized that a direct wind forced process leads to thermocline shallowing in the central and eastern Pacific, which affects the SST anomaly. However, they focused only on direct forcing of the equatorial wind stress and did not explain the ocean adjustment brought by the anomalous mass transport.

[48] The intermediate model experiments in section 4 may give a clue in relation to this question. The amplitude of the model-produced SST becomes slightly larger and the period becomes more regular when the wind stress pattern becomes symmetric, although the differences are small. Wind stress forcing on the equator rather than on the off-equator region is more effective in inducing a thermocline depth anomaly in the equatorial eastern Pacific that can strongly affect SST. Thus an antisymmetric wind stress about the equator may produce a relatively weak SST anomaly compared to that associated with a symmetric wind stress. Also, the antisymmetry of the wind stress can affect the ENSO timescale because the period is related to the timescale of meridional mass exchange. As mentioned in section 3, the meridional shift of the zonal wind stress induces inefficient mass transport. Note that the atmosphere model produces a wind stress based on the empirical relation between the observed SST and the wind stress. This means that our intermediate model experiments might underestimate the impact of the wind stress shift. In order to examine the impact of the wind stress shift, models that support active air-sea interaction and feedback are needed.

Appendix A

[49] By using a Taylor expansion, equation (1) in text can be approximated by the following equation:

$$\tau_x(x,y) \approx A(x)\exp\left[-\frac{y^2}{Y_c^2}\right]\exp\left[-\frac{y_0^2}{Y_c^2}\right]\left(1-\frac{2yy_0}{Y_c^2}\right). \qquad \text{(A1)}$$

[50] First of all, we separate the wind stress pattern into its symmetric and antisymmetric components about the equator. The symmetric component of wind stress is defined as $(\tau_{NH} + \tau_{SH})/2$, which induces symmetric mass transport about the equator, and the antisymmetric component is defined as $(\tau_{NH} - \tau_{SH})/2$. According to these definitions, equation (A1) is separated as follows:

$$\text{Symetric part}: \tau_s(x,y) = B\exp\left[-\frac{y^2}{Y_c^2}\right]$$

$$\text{Antisymetric part}: \tau_a(x,y) = -B\left(\frac{2yy_0}{Y_c^2}\right)\exp\left[-\frac{y^2}{Y_c^2}\right] = -\left(\frac{2yy_0}{Y_c^2}\right)\tau_s, \qquad \text{(A2)}$$

where

$$B = A(x)\exp\left[-\frac{y_0^2}{Y_c^2}\right].$$

[51] By substituting equation (A2) into equation (1), we can obtain the formulae for the Ekman and Sverdrup transports due to the symmetric and antisymmetric wind components.

[52] **Acknowledgments.** J.-S. Kug and I.-S. Kang were supported by the Climate Environment System Research Center sponsored by Korea Science and Engineer Foundation and the BK21 project of the Korean Government. S.-I. An has been supported by Frontier Research System for Global Change through its sponsorship of the International Pacific Research Center (IPRC). This study was funded by School of Ocean and Earth Science and Technology contribution 6173 and International Pacific Research Center contribution IPRC-214.

References

Acero-Schertzer, C. E., D. V. Hansen, and M. S. Swenson, Evaluation and diagnosis of surface currents in the National Centers for Environmental Prediction's ocean analyses, *J. Geophys. Res.*, *102*, 21,037–21,048, 1997.

An, S.-I., and I.-S. Kang, A further investigation of the recharge oscillator paradigm for ENSO using a simple coupled model with the zonal mean and eddy separated, *J. Clim.*, *13*, 1987–1993, 2000.

An, S.-I., and I.-S. Kang, Tropical Pacific basin-wide adjustment and oceanic waves, *Geophys. Res. Lett.*, *28*, 3975–3978, 2001.

Behringer, D. W., M. Ji, and A. Leetmaa, An improved coupled model for ENSO prediction and implication for ocean initialization, part I, The ocean data assimilation system, *Mon. Weather Rev.*, *126*, 1013–1021, 1998.

Bjerknes, J., Atmospheric teleconnections from the equatorial Pacific, *Mon. Weather Rev.*, *97*, 163–172, 1969.

Cane, M. A., and D. W. Moore, A note on low-frequency equatorial basin modes, *J. Phys. Oceanogr.*, *11*, 1578–1584, 1981.

Cane, M. A., and E. S. Sarachik, The response of a linear baroclinic equatorial ocean to periodic forcing, *J. Mar. Res.*, *39*, 651–693, 1981.

Cassou, C., and C. Perigaud, ENSO simulated by intermediate models and evaluated with observations over 1970–1998, part II, Role of the off-equatorial ocean and meridional winds, *J. Clim.*, *13*, 1635–1663, 2000.

Gill, A. E., *Atmosphere-Ocean Dynamics*, Academic, San Diego, Calif., 1982.

Harrison, D.-E., and G. A. Vecchi, On the termination of El Niño, *Geophys. Res. Lett.*, *11*, 1593–1596, 1999.

Ji, M., A. Leetmaa, and J. Derber, An ocean analysis system for seasonal to interannual climate studies, *Mon. Weather Rev.*, *123*, 460–481, 1995.

Jin, F.-F., An equatorial ocean recharge paradigm for ENSO, part I, Conceptual model, *J. Atmos. Sci.*, *54*, 811–829, 1997a.

Jin, F.-F., An equatorial ocean recharge paradigm for ENSO, part II, A stripped-down coupled model, *J. Atmos. Sci.*, *54*, 830–847, 1997b.

Kang, I.-S., and J.-S. Kug, An El-Niño prediction system with an intermediate ocean and statistical atmosphere model, *Geophys. Res. Lett.*, *27*, 1167–1170, 2000.

Kirtman, B. P., Oceanic Rossby wave dynamics and the ENSO period in a coupled model, *J. Clim.*, *10*, 1690–1704, 1997.

Kirtman, B. P., and S. E. Zebiak, ENSO simulation and prediction with a hybrid coupled model, *Mon. Weather Rev.*, *125*, 2620–2641, 1997.

Meinen, C. S., and M. J. McPhaden, Observations of warm water volume changes in the equatorial Pacific and their relationship to El Niño and La Niña, *J. Clim.*, *13*, 3551–3559, 2000.

Meinen, C. S., and M. J. McPhaden, Interannual variability in warm water volume transports in the equatorial pacific during 1993–1999, *J. Phys. Oceanogr.*, *31*, 1324–1345, 2001.

Meinen, C. S., and D. R. Watts, Vertical structure and transport on a transect across the North Atlantic current near 42°: Time series and mean, *J. Geophys. Res.*, *105*, 21,869–21,892, 2000.

Perigaud, C., F. Melin, and C. Cassou, ENSO simulated by intermediate models and evaluated with observations over 1970–1998, part I, Role of the off-equatorial variability, *J. Clim.*, *13*, 1605–1634, 2000.

Rasmusson, E. M., and T. H. Carpenter, Variations in tropical sea surface temperature and surface wind fields associated with the Southern Oscillation/El Niño, *Mon. Weather Rev.*, *110*, 354–384, 1982.

Smith, N. R., An improved system for tropical ocean subsurface temperature analyses, *J. Atmos. Oceanic Technol.*, *12*, 850–870, 1995.

Vossepoel, F. C., and D. W. Behringer, Impact of sea level assimilation on salinity variability in the western equatorial Pacific, *J. Phys. Oceanogr.*, *30*, 1706–1721, 2000.

Wang, B., and Z. Fang, Chaotic oscillation of the tropical climate: A dynamic system theory for ENSO, *J. Atmos. Sci.*, *53*, 2786–2802, 1996.

Wang, B., R. Wu, and R. Lukas, Roles of the western North Pacific wind variation in thermocline adjustment and ENSO phase transition, *J. Meteorol. Soc. Jpn.*, *77*, 1–16, 1999.

Wyrtki, K., El Niño—The dynamic response of equatorial Pacific Ocean to atmospheric forcing, *J. Phys. Oceanogr.*, *5*, 572–584, 1975.

Wyrtki, K., Water displacements in the Pacific and the genesis of El Niño cycles, *J. Geophys. Res.*, *90*, 7129–7132, 1985.

Yu, J.-Y., and C. R. Mechoso, Coupled atmosphere-ocean GCM study of the ENSO cycle, *J. Clim.*, *14*, 2329–2350, 2001.

Zebiak, S. E., and M. A. Cane, A model El Niño-Southern oscillation, *Mon. Weather Rev.*, *115*, 2262–2278, 1987.

S.-I. An, International Pacific Research Center, SOEST, University of Hawaii at Manoa, Honolulu, HI, USA.

I.-S. Kang, School of Earth and Environmental Sciences, Seoul National University, Seoul 151-742, Korea. (kang@climate.snu.ac.kr)

J.-S. Kug, Department of Atmospheric Sciences, Seoul National University, Kwanwak-Ku 151-742, Seoul, Korea. (jskug@climate.snu.ac.kr)